BIOCHEMISTRY
including biophysical chemistry & molecular biology
Article

Biochemistry **2011,** *50,* 1247–1254 1247
DOI: 10.1021/bi101642d

Methylthioinosine Phosphorylase from *Pseudomonas aeruginosa*. Structure and Annotation of a Novel Enzyme in Quorum Sensing[†]

Rong Guan,[‡] Meng-Chiao Ho,[‡] Steven C. Almo, and Vern L. Schramm*

Department of Biochemistry, Albert Einstein College of Medicine, Yeshiva University, 1300 Morris Park Avenue, Bronx, New York 10461, United States. [‡]*These authors contributed equally to this work.*

Received October 13, 2010; Revised Manuscript Received December 30, 2010

ABSTRACT: The PA3004 gene of *Pseudomonas aeruginosa PAO1* was originally annotated as a 5′-methylthioadenosine phosphorylase (MTAP). However, the PA3004 encoded protein uses 5′-methylthioinosine (MTI) as a preferred substrate and represents the only known example of a specific MTI phosphorylase (MTIP). MTIP does not utilize 5′-methylthioadenosine (MTA). Inosine is a weak substrate with a k_{cat}/K_m value 290-fold less than MTI and is the second best substrate identified. The crystal structure of *P. aeruginosa* MTIP (*Pa*MTIP) in complex with hypoxanthine was determined to 2.8 Å resolution and revealed a 3-fold symmetric homotrimer. The methylthioribose and phosphate binding regions of *Pa*MTIP are similar to MTAPs, and the purine binding region is similar to that of purine nucleoside phosphorylases (PNPs). The catabolism of MTA in *P. aeruginosa* involves deamination to MTI and phosphorolysis to hypoxanthine (MTA → MTI → hypoxanthine). This pathway also exists in *Plasmodium falciparum*, where the purine nucleoside phosphorylase (*Pf*PNP) acts on both inosine and MTI. Three tight-binding transition state analogue inhibitors of *Pa*MTIP are identified with dissociation constants in the picomolar range. Inhibitor specificity suggests an early dissociative transition state for *Pa*MTIP. Quorum sensing molecules are associated with MTA metabolism in bacterial pathogens suggesting *Pa*MTIP as a potential therapeutic target.

Pseudomonas aeruginosa is a Gram-negative bacterium found in a wide range of environments including water, soil, and mammals (*1*). It is a major opportunistic human pathogen, infecting burns and lungs in cystic fibrosis (*2*). Compromised immune systems and extended hospitalization are correlated with infections, making *P. aeruginosa* the causative agent of approximately 15% of all hospital infections (*2*). *P. aeruginosa* infections are difficult to treat since the bacterium has multiple antimicrobial resistance mechanisms (*3*). Chronic infections can be severe in patients with cystic fibrosis, causing high rates of morbidity and mortality (*4*, *5*). *P. aeruginosa* contains quorum sensing (QS)[1] pathways involved in the regulation of virulence factors and biofilm formation (*7*). Signal molecules of QS include *N*-acylhomoserine lactones (AHLs). The concentration of AHLs increases during bacterial growth to allow AHL binding to specific receptors with the regulation of target genes. In *P. aeruginosa*, the *las* and *rhl* QS systems use AHLs of 3-oxo-C_{12}-homoserine lactone and C_4-homoserine lactone as signal molecules, respectively. Microarray studies on *P. aeruginosa* indicated that QS regulated 3−7% of the total open reading frames (*6*−*8*). Deletion of single or multiple QS genes reduced the virulence of *P. aeruginosa* in mouse studies, indicating a strong correlation between the QS system and *P. aeruginosa* pathogenesis (*9*−*14*). Quorum sensing blockade does not affect bacterial growth and is therefore expected to attenuate the virulence of infection without causing drug resistance (*15*).

Potential therapeutic targets in the QS system include enzymes involved in the formation of AHLs that act as signaling molecules and as virulence factors in *P. aeruginosa* (*15*). AHLs are synthesized from *S*-adenosylmethionine (SAM) and acylated acyl carrier protein by AHL synthase with 5′-methylthioadenosine (MTA) as a byproduct. MTA is recycled to ATP and methionine for SAM recycling (*16*). In bacteria, 5′-methylthioadenosine nucleosidase (MTAN) is part of the normal pathway to produce adenine and 5-methylthioribose α-D-1-phosphate (MTR-1-P) from MTA for SAM recycling. Transition-state analogue inhibitors of *Escherichia coli* and *Vibrio cholerae* MTAN disrupt quorum sensing and reduce biofilm formation, supporting MTAN as a target for QS (*16*).

P. aeruginosa is an unusual bacterium as it possesses a putative 5′-methylthioadenosine phosphorylase (MTAP: PA3004 gene) instead of MTAN. MTAP is rare in bacteria and common in mammals while MTAN is not found in mammals. The action of MTAP on MTA would be functionally similar to that of MTAN by relieving MTA product inhibition of AHL synthase and permitting SAM recycling in *P. aeruginosa* (*17*).

The PA3004 gene of *P. aeruginosa PAO1* encodes a protein (NCBI ID NP_251694.1) annotated as a "probable nucleoside phosphorylase" in pseudoCAP (*18*). It was later proposed to be an MTAP based on catabolism studies in mutant strains of

[†]This work was supported by NIH Research Grant GM41916.

*Corresponding author. Telephone: 718-430-2813. Fax: 718-430-8565. E-mail: vern.schramm@einstein.yu.edu.

[1]Abbreviations: MTA, 5′-methylthioadenosine; MTI, 5′-methylthioinosine; QS, quorum sensing; AHLs, *N*-acylhomoserine lactones; MTAP, MTA phosphorylase; MTIP, MTI phosphorylase; PNP, purine nucleoside phosphorylase; MTAN, MTA nucleosidase; MTR-1-P, 5-methylthioribose α-D-1-phosphate; SAM, *S*-adenosylmethionine; ImmH, immucillin-H; MT-ImmH, 5′-methylthio-ImmH; PhT-ImmH, 5′-phenylthio-ImmH; ImmA, immucillin-A; DADMe, 4′-deaza-1′-aza-2′-deoxy-1′-(9-methylene); MT-DADMe-ImmH, 5′-methylthio-DADMe-ImmH.

Published on Web 01/03/2011

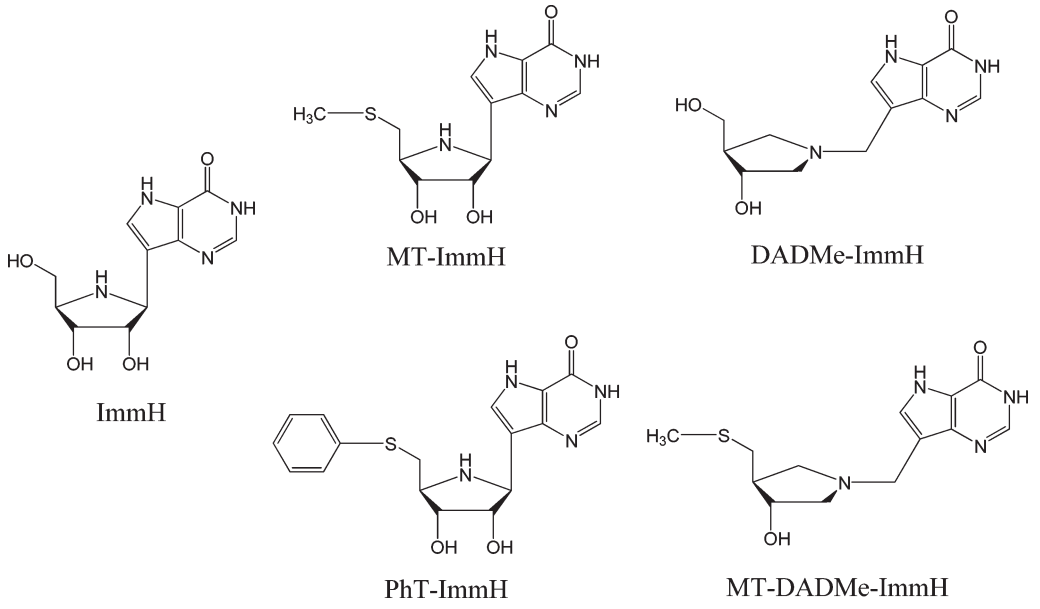

FIGURE 1: Early and late transition-state mimics as inhibitors for *Pa*MTIP and *Pf*PNP.

P. aeruginosa (*19*). PAO503 is a *P. aeruginosa* methionine auxotroph. A new strain (PAO6422) was created by inactivating the PA3004 gene of PAO503. PAO503 was complemented for growth on minimum medium with methionine, homocysteine, or MTA. PAO6422 responded to methionine and homocysteine but was not complemented by MTA (*19*). These results supported an MTAP activity for the PA3004 encoded protein. However, the results also support a pathway of MTA → MTI → hypoxanthine + MTR-1-P → methionine, but this was not considered in the original annotation.

In this report we establish the PA3004 encoded protein to be 5′-methylthioinosine phosphorylase (MTIP). Examination of MTA metabolism in *P. aeruginosa* using [8-^{14}C]MTA confirmed that the pathway involves MTIP. The crystal structure of *Pa*MTIP and three transition-state analogue inhibitors with picomolar K_i values for *Pa*MTIP are described.

MATERIALS AND METHODS

Chemicals. MT-ImmH, PhT-ImmH, and MT-DADMe-ImmH were synthesized by the Carbohydrate Chemistry Team of Industrial Research Ltd., Lower Hutt, New Zealand (Figure 1). [8-^{14}C]MTA was synthesized as described previously (*20*). All other chemicals and reagents were obtained from Sigma or Fisher Scientific and were of reagent grade.

Plasmid Construction. A synthetic gene was designed based on the predicated protein sequence of NP_251694.1 in NCBI, annotated as MTAP of *P. aeruginosa PAO1*. The synthetic gene was obtained in a pJexpress414 expression vector from DNA2.0 Inc. This construct encodes an additional 14 amino acids at the N-terminus which includes a His_6 tag and a TEV cleavage site.

Enzyme Purification and Preparation. BL21-CodonPlus-(DE3)-RIPL *E. coli* were transformed with the above plasmid and grown overnight at 37 °C in 50 mL of LB medium with 100 μg/mL ampicillin. The culture was transferred into 1 L of LB/ampicillin medium, and growth continued at 37 °C to an OD_{600} of 0.7. Expression was induced by addition of 1 mM IPTG. After 4 h at 37 °C, the cells were harvested by centrifugation at 4500*g* for 30 min. The cell pellet was suspended in 20 mL of 15 mM imidazole, 300 mM NaCl, and 50 mM phosphate, pH 8.0 (lysis buffer), with two tablets of EDTA-free protease inhibitor (from Roche Diagnostics) and lysozyme (from chicken egg) added to the mixture. Cells were disrupted twice with a French press and centrifuged at 20000*g* for 30 min. The supernatant was loaded onto a 4 mL column of Ni-NTA Superflow resin previously equilibrated with five columns of lysis buffer. The column was washed with 5 volumes of 80 mM imidazole, 300 mM NaCl, and 50 mM phosphate, pH 8.0 (wash buffer), and enzyme was eluted with 3 volumes of 250 mM imidazole, 300 mM NaCl, and 50 mM phosphate, pH 8.0 (elution buffer). The purified enzyme (> 95% purity on the basis of SDS−PAGE) was dialyzed against 50 mM Hepes, pH 7.4, and concentrated to 8 mg/mL. Enzyme was stored at −80 °C. The extinction coefficient of *Pa*MTIP is 20.4 mM^{-1} cm^{-1} at 280 nm, determined by the ProtParam program from ExPASy (http://ca.expasy.org/seqanalref/).

Enzymatic Assays. Product formation was monitored by conversion of hypoxanthine to uric acid by xanthine oxidase (*21*). The extinction coefficient for conversion of MTI to uric acid was 12.9 mM^{-1} cm^{-1} at 293 nm. Enzyme activity with adenosine or MTA as substrates was determined by conversion of adenine to 2,8-dihydroxyadenine using xanthine oxidase as the coupling enzyme (*22*). The extinction coefficient for conversion of adenosine or MTA to 2,8-dihydroxyadenine at 293 nm was 15.2 mM^{-1} cm^{-1}. Reactions were carried out at 25 °C in 1 cm cuvettes, 1 mL volumes of 100 mM Hepes, pH 7.4, and 100 mM phosphate, pH 7.4, variable concentrations of nucleoside substrate, 0.5 unit of xanthine oxidase, 5 mM DTT, and appropriate amounts of purified MTIP. Reactions were initiated by addition of enzyme, and the initial rates were monitored with a CARY 300 UV−visible spectrophotometer. Control rates (no *Pa*MTIP) were subtracted from initial rates. K_m and k_{cat} values for *Pa*MTIP were obtained by fitting initial rates to the Michaelis−Menten equation using GraFit 5 (Erithacus Software). Phosphate was found to be near saturation when present at 100 mM.

Inhibition Assays. Assays for slow-onset inhibitors were carried out by adding 1 nM *Pa*MTIP into reaction mixtures at 25 °C containing 100 mM Hepes, pH 7.4, 100 mM phosphate, pH 7.4, 2 mM MTI, 5 mM DTT, 0.5 unit of xanthine oxidase, and variable inhibitor concentration. Inhibitors were present at ≥10 times the enzyme concentration, required to simplify data

analysis (*23*). Assays for MTA inhibition used 200 μM MTI. Controls having no enzyme and no inhibitor were included in all of the inhibition assays. Inhibition constants were obtained by fitting initial rates with variable inhibitor concentrations to eq 1 using GraFit 5 (Erithacus Software):

$$\frac{v_i}{v_0} = \frac{K_m + [S]}{K_m + [S] + \frac{K_m[I]}{K_i}} \quad (1)$$

where v_i is the initial rate in the presence of inhibitor, v_0 is the initial rate in the absence of inhibitor, K_m is the Michaelis constant for MTI, [S] and [I] are MTI and inhibitor concentrations, respectively, and K_i is the inhibition constant. Tight-binding inhibitors often display two phases of binding. After the initial rate, a second phase of tighter binding is achieved and results in more potent inhibition. The dissociation constant for the second binding phase is indicated as K_i*. This constant was obtained by fitting reaction rates achieved following slow-onset inhibition and inhibitor concentrations to eq 1 using GraFit 5, but where K_i is replaced by K_i* (*21*).

Protein Crystallization and Data Collection. Recombinant *Pa*MTIP (9 mg/mL) in 50 mM HEPES, pH 7.4, crystallized in 30% polyethylene glycol monomethyl ether 2000 and 0.1 M potassium thiocyanate in the presence of 5 mM MTI and 5 mM sulfate by sitting-drop vapor diffusion. Crystals were transferred to a fresh drop of crystallization solution supplemented with 20% glycerol and flash-cooled in liquid nitrogen. X-ray diffraction data were collected at Beamline X29A, Brookhaven National Laboratory, and processed with the HKL2000 program suite (Table 1).

Structure Determination and Refinement. The crystal structure of *Pa*MTIP was determined by molecular replacement with Molrep using the published structure of *Sulfolobus tokodaii* MTAP (PDB ID 1V4N, 33.7% sequence identity) as the search model (*24*). A model without catalytic site ligands was built by Phenix (*25*), followed by iterative rounds of manual model building and refinement in COOT and REFMAC5 (*26*, *27*). Although *Pa*MTIP was cocrystallized in the presence of sulfate and MTI to mimic the Michaelis complex of *Pa*MTIP, based on ligand-omitted $F_o - F_c$ maps (contoured at 3σ) electron density was consistent with the presence of only a purine ring in the active site (Figure 2). *Pa*MTIP was later confirmed to hydrolyze MTI under these conditions. Thus, hypoxanthine was modeled in the active site of *Pa*MTIP (Table 1).

MTA Catabolism Using [8-^{14}C]MTA. *P. aeruginosa PAO1* (ATCC number 15692) was grown at 37 °C in LB medium for 16 h. Cells were collected by centrifugation at 16100*g* and washed twice with 100 mM phosphate, pH 7.4. Washed cells were lysed using BugBuster (Novagen). Cleared lysate (53 μL) was incubated with [8-^{14}C]MTA (10 μL containing approximately 0.1 μCi of ^{14}C) in 100 mM phosphate, pH 7.4, for 10 and 25 min. Reaction mixtures were quenched with perchloric acid (1.8 M final concentration) and neutralized with potassium hydroxide. Precipitates were removed by centrifugation, and carrier hypoxanthine, adenine, MTI, and MTA were added to the cleared supernatant. Metabolites were resolved on a C_{18} Luna HPLC column (Phenomenex) with a gradient of 5−52.8% acetonitrile in 20 mM ammonium acetate, pH 5.2. UV absorbance was detected at 260 nm, and the retention times were 5.1 min for hypoxanthine, 7.5 min for adenine, 20.4 min for MTI, and 21.9 min for MTA. Fractions were collected in scintillation vials, dried, and reconstituted in 200 μL of deionized water prior to addition of 10 mL of ULTIMA GOLD LSC-Cocktail, and ^{14}C was counted for three cycles at 20 min per cycle using a Tri-Carb 2910TR liquid scintillation analyzer. Control experiments replaced cell lysate by lysis buffer in reaction mixtures.

Table 1: Data Collection and Refinement Statistics[a]

data collection	
PDB	3OZB
space group	$P4_12_12$
cell dimension	
a, *b*, *c* (Å)	99.5, 99.5, 334.9
α, *β*, *γ* (deg)	90.0, 90.0, 90.0
resolutions (Å)	20.0−2.8 (2.9−2.8)
R_{sym} (%)	17.2 (95.5)
$I/\sigma I$	9.6 (1.9)
completeness (%)	100.0 (100.0)
redundancy	7.0 (7.2)
refinement	
resolution (Å)	20.00−2.8
no. of reflections	42041
R_{work}/R_{free} (%)	20.2/26.2
B-factors (Å^2)	
protein (main chain)	39.9
protein (side chain)	40.9
water	25.1
ligand	45.7
no. of atoms	
protein	10800
water	63
ligand	60
rms deviations	
bond lengths (Å)	0.012
bond angles (deg)	1.47
Ramachandran analysis	
allowed region (%)	99.3
disallowed region (%)	0.7

[a]Numbers in parentheses are for the highest resolution shell. One crystal was used for each data set.

RESULTS AND DISCUSSION

PA3004 Encodes a MTI Phosphorylase. The recombinant protein from PA3004 was purified and tested for substrate specificity (Table 2). The recombinant protein did not utilize MTA in the presence or absence of phosphate ($< 10^{-4}$ s^{-1}). The most favorable reaction was phosphorolysis of MTI with a k_{cat} of 4.8 s^{-1} and a K_m of 2.6 μM (k_{cat}/K_m of 1.8×10^6 M^{-1} s^{-1}). Enzyme was less active with inosine with a k_{cat} of 0.57 s^{-1} and a K_m of 90 μM (k_{cat}/K_m of 6×10^3 M^{-1} s^{-1}). The methylthio group of MTI is important for both substrate binding and catalysis. Adenosine is a weak substrate with a k_{cat} of 0.0549 s^{-1} and a K_m of 23 μM (k_{cat}/K_m of 2.4×10^3 M^{-1} s^{-1}). Thus the protein encoded by PA3004 is a relatively specific MTI phosphorylase. The catalytic efficiency (k_{cat}/K_m) for MTI is 290 times larger than for inosine, the second best substrate. For comparison, the MTI phosphorylase activity of *Pf*PNP (see below) has a k_{cat}/K_m of 9.4×10^4 M^{-1} s^{-1} for MTI and a k_{cat}/K_m of 3.6×10^5 M^{-1} s^{-1} for inosine.

MTIP of *P. aeruginosa* is the only known example of a specific MTI phosphorylase. MTA is not a substrate ($< 10^{-4}$ s^{-1} k_{cat}) but is a competitive inhibitor of MTI, with a K_i value of 70 μM, three times greater than the K_m of adenosine. Thus, MTA binds to the active site of the enzyme but is not catalytically competent. MTIP activity has been reported in *Caldariella acidophilan* MTAP, human MTAP, human PNP, and *Plasmodium falciparum* PNP, but MTI is a relatively poor substrate for these enzymes (*28*−*31*).

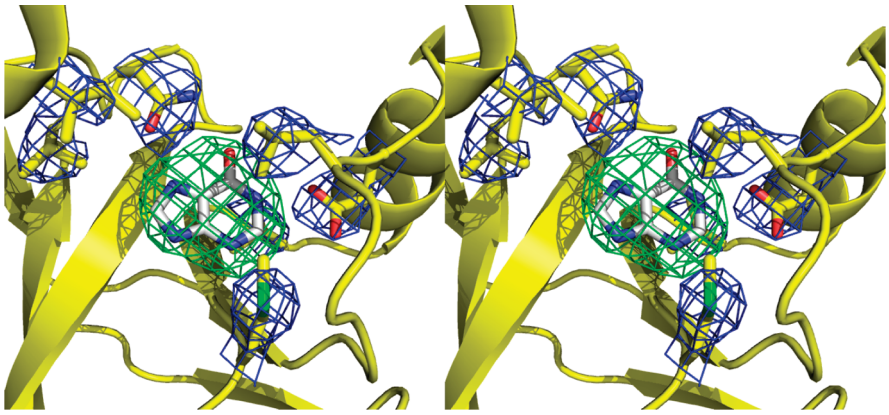

FIGURE 2: Stereoview of the hypoxanthine-omitted electron density map of *Pa*MTIP in complex with hypoxanthine. The residues interacting with hypoxanthine are shown as yellow sticks and overlaid with a $2mF_o - DF_c$ electron density map (contour at 1σ). Hypoxanthine carbons are shown as gray sticks and overlaid with a $mF_o - DF_c$ electron density map (contour at the 3σ).

Table 2: Substrate Specificity of *Pa*MTIP[c]

substrate	k_{cat} (s^{-1})	K_m or K_i (μM)	k_{cat}/K_m (M^{-1} s^{-1})
MTI	4.8 ± 0.2	2.6 ± 0.4	$(1.8 \pm 0.3) \times 10^6$
MTA[a]	N/A	70 ± 20	N/A
inosine	0.57 ± 0.04	90 ± 20	$(6 \pm 1) \times 10^3$ [300][b]
adenosine	0.0549 ± 0.0005	23 ± 1	$(2.4 \pm 0.1) \times 10^3$ [750][b]

[a]MTA is not a substrate of *Pa*MTIP. K_i is used instead of K_m for MTA. [b]Numbers in brackets are fold decreases of k_{cat}/K_m in comparison with those of MTI. [c]Values are ±SE.

Recombinant MTIP was expressed with a 14 amino acid extension at the N-terminus. Incubation with TEV protease removed 13 of these, leaving one additional glycine at the N-terminus. This construct exhibited the same kinetic properties as the original recombinant protein. The crystal structure (see below) shows the N-terminal extension to be remote from the active site.

Crystal Structure of PaMTIP:Hypoxanthine. The crystal structure of *Pa*MTIP in complex with hypoxanthine was determined to 2.8 Å resolution with two homotrimers in the asymmetric unit. Residues 2−54 and 60−243 of each *Pa*MTIP monomer are ordered in the electron density map. The N-terminal His_6 tag and TEV protease site are disordered and distant from the active site. The *Pa*MTIP monomer is folded into a single domain structure including ten β strands and five α helices (Figure 3A). The core consists of a mixed seven-stranded β sheet (β2, β3, β4, β1, β5, β10, and β6) which is flanked by five α helices. β5 is extended and participates in an additional four-stranded β sheet (β5, β9, β8, and β7) (Figure 3A).

The active sites of *Pa*MTIP are located near the interfaces formed between monomers in the trimer. Each trimeric *Pa*MTIP forms three active sites (Figure 3B). Although *Pa*MTIP was cocrystallized with MTI and sulfate (5 mM) to mimic the Michaelis complex, the ligand-omitted difference Fourier map showed only the presence of hypoxanthine (Figure 2). Kinetic experiments demonstrated slow hydrolysis of MTI (3.8×10^{-5} s^{-1}) to generate hypoxanthine and 5-methylthioribose. Crystallization attempts with apo-*Pa*MTIP or with *Pa*MTIP in complex with hypoxanthine and phosphate failed to yield crystals. In the crystal structure, hypoxanthine is wedged between the backbone of a four-stranded β sheet and the side chains of Leu180 and Met190. Structure-based sequence alignment revealed that Met190 is conserved and Leu180 is replaced by Phe in human PNP and human MTAP (Figure 4). Hypoxanthine N7 and O6 form hydrogen bonds with the side chain of Asn223 in *Pa*MTIP, and N1 forms a hydrogen bond with the side chain of Asp181 (Figure 2).

Comparison with Other Purine N-Ribosylphosphorylases. Similar catalytic chemistries to *Pa*MTIP are found in the PNPs and MTAPs. It is of interest to examine the amino acid sequences that distinguish *Pa*MTIP and permit its unique substrate specificity. The sequence differences are also useful for identification of other MTIPs in sequence databases.

The trimeric subunit structure of *Pa*MTIP is similar to the four trimeric MTAPs and seven trimeric PNPs in the Protein Data Bank (rmsd is in the range of 0.8−1.2 Å for the monomers). Structure-based sequence alignments with *Pa*MTIP show a 28−40% identity with the four MTAPs and 20−32% with the seven trimeric PNPs (Figure 4). Ironically, the enzyme most closely related to *Pa*MTIP in catalytic activity is the hexameric *P. falciparum* PNP/MTIP, but it shows no significant similarity in amino acid sequence or quaternary structures with the trimeric PNPs, MTAPs, and *Pa*MTIP. Because of these distinct features, *Plasmodium* PNPs are not included in the following structural analysis (*32*).

The active sites of *Pa*MTIP, PNPs, and MTAPs can be divided into three distinct regions corresponding to the purine, (methylthio)ribose and phosphate binding regions. Glu201 and Asn243 (human PNP numbering) are conserved in the purine binding region of *Pa*MTIP and PNPs (Figure 4) and have important roles in 6-oxopurine specificity by hydrogen bonding to N1, O6, and N7 of the 6-oxopurine (Figure 5A) (*33*). The Asn243Asp mutant and Glu201Gln:Asn243Asp double mutant in human PNP are known to shift the substrate preference in favor of adenosine, a 6-aminopurine substrate and a preferred substrate for MTAP (*34*). MTAPs prefer 6-aminopurine groups because Asp222 (human MTAP numbering, Figure 5C) forms two favorable hydrogen bonds with the N6 amino group and with N7 of the purine ring (*29*). The ribose binding region of human PNP prefers nucleosides with a 5′-hydroxyl group but not a 5′-methylthio group. The conserved His257 and Phe159 (from the adjacent monomer) of human PNP are important in binding the 5′-hydroxyl group. His257 forms a H-bond to the 5′-hydroxyl group, and catalytic efficiency drops by 660 in His257Gly (*38*). In MTAP and *Pa*MTIP, a small hydrophobic amino acid corresponding to His257 of human PNP and a histidine corresponding to Phe159 (human PNP numbering) provide space to accommodate the 5′-methylthio group (Figure 5). Consistent with these

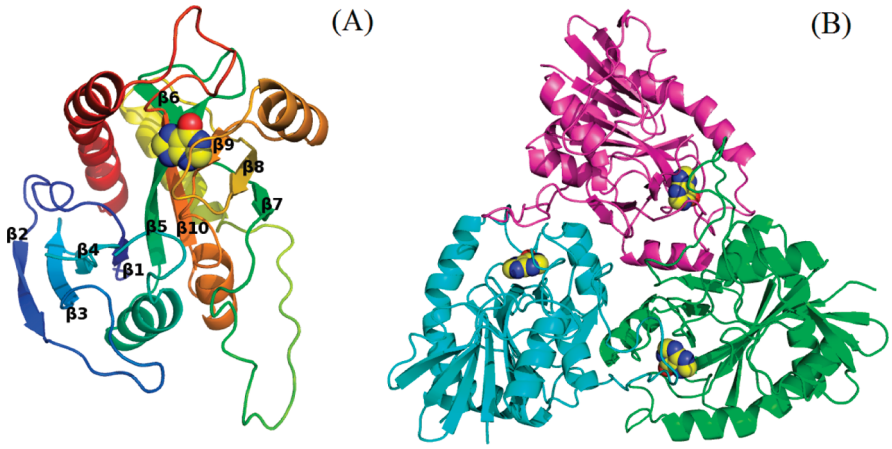

FIGURE 3: Crystal structure of *Pa*MTIP. (A) A view of the *Pa*MTIP monomer looking toward the catalytic site. The structure is colored from blue (N-terminus) to red (C-terminus). Hypoxanthine is included as a space-filling model to show the position of the active site. (B) The monomers of trimeric *Pa*MTIP are shown in blue, green, and magenta. Hypoxanthine is included as space-filling models.

```
1YR3   6 -FSHNPLFCIDIIKTYKPD-FTPRVAFILGSGLGALAD-QIENAVAISYEKLPGFPVSTVHGHAGELVLGHLQGVPVVCMKGR------GHFYEGRGM
1N3I   9 --DELARRAAQVIADRTG-IGEHDVAVVLGSGWLPAVAALGSPTTVLPQAELPGFVPPTAAGHAGELLSVPIGAHRVLVLAGR------IHAYEGHDL
3KHS   3 -DYDLAKETAAWLNKQLQ--IRPVLGIVCGSGLGKIGD-SLETSITVAYSDIPNFPVGSVKGHAGSLIFGSVNGVSCVCMKGR------FHLYEGHTA
2P4S  90 YTYDTLQEIATYLLERTE--LRPKVGIICGSGLGTLAE-QLTDVDSFDYETIPHFPVSTVAGHVGRLVFGYLAGVPVMCMQGR------FHHYEGYPL
1VMK   1 -MMKKIEEARTFISERTN--LSPDILIILGSGFGPFIE-KVEDPVIIDYKDIPHFPQPTVEGHSGKLVFGRISDKPVMIMAGR------FHLYEGHDP
1A9T   5 YTYEDYQDTAKWLLSHTE--QRPQVAVICGSGLGGLVN-KLTQAQTFDYSEIPNFPESTVPGHAGRLVFGILNGRACVMMQGR------FHMYEGYPF
1RR6   5 YTYEDYKNTAEWLLSHTK--HRPQVAIICGSGLGGLTD-KLTQAQIFDYSEIPNFPRSTVPGHAGRLVFGFLNGRACVMMQGR------FHMYEGYPL
3OZB  17 ----------------------VYAIIG---GTGLTQLEGLTLSESL---PIETPYGAPS---APLQRGRYAGREVLFLARHGHPHRFPPHQV----
1V4N   7 --------------------EKASIGIIG---GSGLYDPQILTNVKEI---KVYTPYGEPS---DNIILGELEGRKVAFLPRHGRGHRIPPHKI----
1K27  11 ----------------------KIGIIGGTGLDD-PE--ILEGRTEK---YVDTPFGKPS---DALILGKIKNVDCVLLARHGRQHTIMPSKV----
1WTA   3 ---------EITR--PPG--VRAHVGVIG---GSGLYDPGIVENPVEV---KVSTPYGNPS---DFIVVGDVAGVKVAFLPRHGRGHRIPPHAI----
2A8Y   2 ----------IEQN------EKASIGIIGGGSGLYDP-G--IFSESKEI---KVYTPYGQPS---DFITIGKIGNKSVAFLPRHGRGHRIPPHKI----

1YR3  95 TIMTDAIRTFKLLGCELLFCTNAAGSLRPEVGAGSLVALKDHINTM---PGTPMVGL-NDDRFGERFFSLANAYDAEYRALLQKVAKEEGFP--LTEG
1N3I  98 RYVVHPVRAARAAGAQIMVLTNAAGGLRADLQVGQPVLISDHLNLTA---RSPLVGG--------EFVDLTDAYSPRLRELARQSDP------QLAEG
3KHS  91 ARATFPMRVFKALGVKIVVLTNAAGGLNPSYRPGDFMVVRDHINLPGLAGANPLTGP-NDDTEGERFPSMTSVYDKTLRKYAISAARELGMSYATHEG
2P4S 179 AKCAMPVRVMHLIGCTHLIATNAAGGANPKYRVGDIMLIKDHINLMGFAGNNPLQGP-NDERFGPRFFGMANTYDPKLNQQAKVIARQIGIENELREG
1VMK  89 ATVAFPVYLAKYVGVKGVVVTNAAGAINPEFKPGEIILVRDIINFMF---RNPLRGP-NDEKIGPRFPDMSSVVDPEWARKIQERLS-------LKEG
1A9T  94 WKVTFPVRVFRLLGVETLVVTNAAGGLNPNFEVGDIMLIRDHINLPGFSGENPLRGP-NEERFGVRFPAMSDAYDRDMRQKAHSTWKQMGEQRELQEG
1RR6  94 WKVTFPVRVFHLLGVDTLVVTNAAGGLNPKFEVGDIMLIRDHINLPGFSGQNPLRGP-NDERFGDRFPAMSDAYDRTMRQRALSTWKQMGEQRELQEG
3OZB  79 -NYRANLWALKQAGAEAVIAVNAVGGIHAAMGTGHLCVPHQLIDYTSG-REHTYFAG---DIEHVTHIDFSHPYDPELRQRLIEALRALGL-AHSSHG
1V4N  72 -NYRANIWALKSLGVKWVIAVSAVGSLRLDYKPGDFVVPNQFIDMTKG-RTYTFFDG-----PTVAHVSMADPFCEHLRSIILDSAKDLGI-TTHDKG
1K27  73 -NYQANIWALKEEGCTHVIVTTACGSLREEIQPGDIVIIDQFIDRTTM-RPQSFYDGSHSCARGVCHIPMAEPFCPKTREVLIETAKKLGL-RCHSKG
1WTA  75 -NYRANIWALKALGVKWVISVSAVGSLREDYRPGDFVVPDQFIDMTKNRRHYTFYD-----GPVTVHVSMADPFCEDLRQRLIDSGRRLGY-TVHERG
2A8Y  71 -NYRANIWALKELGVRWVISVSAVGSLRMDYKLGDFVIPDQFIDMTKN-REYSFFD-----GPVVAHVSMADPFCNSLRKLAIETAKELNI-KTHESG

1YR3 190 VFVSYPGPNFETAAEIRMMQI-IGGDVVGMSVVPEVISARHCDLKVVAVSAITNMAEGL--SDVKLSHAQTLAAAELSKQNFINLICGFLRKIA---
1N3I 182 VYAGLPGPHYETPAEIRMLQT-LGADLVGMSTVHETIAARAAGAEVLGVSLVTNLAAGI--TGEPLSHAEVLAAGAASATRMGALLADVIARF----
3KHS 191 VYCCVNGPSFETPAECKILRL-MGSDAVGMSTAPETIVAKHGGMRCLAVSLISNVIASNCETPAEPTHEEVLRAGEEASARMTALVKLVIEKIRGE-
2P4S 279 VYTCLGGPNFETVAEVKMLSM-LGVDAIGMSTVHEIITARHCGMTCPAFSLITNMCTMSYEEEEEHCHDSIVGVGKNREKTLGEFVSRIVKHIHYEA
1VMK 179 VYIGVLGPSYETPAEIRVFEK-LGADLVGMSTVPEVIAAKHCGLKVVVFSCVTNMAAG--ITHGRLSHEEVVRTTKMAQGKIEKALTTAVEVF----
1A9T 194 TYVMLGGPNFETVAECRLLRN-LGADAVGMSTVPEVIVARHCGLRVFGFSLITNKVIMDTESQGKANHEEVLEAGKQAAQKLEQFVSLLMASI----
1RR6 194 TYVMVAGPSFETVAECRVLQK-LGADAVGMSTVPEVIVARHCGLRVFGFSLITNKVIMDYESLEKANHEEVLAAGKQAAQKLEQFVSILMASI----
3OZB 174 VYACTQGPRLETVAEIARLER-DGNDIVGMTGMPEAALARELDLPYACLALVVNPAAG-K-SAGIITMAEIEQALHDGIGKVREVLARVLA------
1V4N 165 TYICIEGPRFSTRAESIVWKEVFKADIIGMTLVPEVNLACEAEMCYSVIGMVTCYDV-F--ADIPVTAEEVTKVMAENTAKVKKLLYEVIRRLP---
1K27 171 TMVTIEGPRFSSRAESFMFRT-WGADVINMTTVPEVVLAKEAGICYASIAMATCYDC-WKEHEEAVSVDRVLKTLKENANKAKSLLLTTIPQIGSTE
1WTA 169 TYVCIEGPRFSTRAESRVWKDVFKADIIGMTLVPEINLACEAQLCYATLAMVTCYDV-W--ADRPVTAEEVERVMISNVERARRMLYDVIPKLAGE-
2A8Y 164 TYICIEGPRFSTRAESRTWREVYKADIIGMTLVPEVNLACEAQMCYATIAMVTCYDV-F--AEIPVTAEEVTRVMAENTEKAKKLLYALIQKLPEKP
```

FIGURE 4: Structure-based sequence alignment. Proteins are listed by PDB ID. The top seven sequences are PNPs, the bottom four sequences are MTAPs, and *Pa*MTIP is 3OZB. The conserved residues in the phosphate binding region of PNPs and MTAPs are shaded in light blue and dark blue, respectively. The conserved residues in the purine binding region of PNPs and MTAPs are shaded in light green and dark green, respectively. The conserved Phe and His in the ribose binding region of PNPs are shaded in yellow. The conserved His and small hydrophobic amino acid in the (methylthio)ribose binding region of MTAPs are shaded in orange. The active site residues conserved in all species are shaded in gray. The Leu of *Pa*MTIP is not conserved to either MTAPs or PNPs and is shaded in pink. The PDB IDs are as follows: 1YR3, *E. coli* PNP II; 1N3I, *Mycobacterium tuberculosis* PNP; 3KHS, *Grouper iridoviurs* PNP; 2P4S, *Anopheles gambia* PNP; 1VMK, *Thermotoga maritime* PNP; 1A9T, bovine PNP; 1RR6, human PNP; 3OZB, *Pa*MTIP; 1V4N, *Sulfolobus tokodaii* MTAP; 1K27, human MTAP; 1WTA, *Aeropyrum pernix* K1 MTAP; 2A8Y, *Sulfolobus solfataricus* MTAP.

observations, the His257Gly mutant of human PNP binds 5′-methylthio inhibitors tighter than the corresponding 5′-hydroxyl inhibitors (*35*).

Structural comparison between human MTAP and PNP reveals two distinct motifs in the phosphate binding region. Favorable hydrogen bonds form between phosphate and the 2′- and 3′-hydroxyl groups of (5′-methylthio)ribose and thereby anchor (5′-methylthio)ribose in the active site. The position of phosphate in human MTAP provides more room to accommodate the 5′-methylthio group than the position of phosphate in human PNP, explaining the preference for the 5′-substituents.

Structure-based sequence alignment shows that (1) *Pa*MTIP and MTAP share key residues in the phosphate and (methylthio)ribose binding regions, (2) *Pa*MTIP and PNP share key residues in the purine binding regions (Figures 4 and 5), and (3) these residues provide an approach to identify MTIP in other species.

[8-^{14}*C*]*MTA Catabolism in P. aeruginosa*. Substrate specificity and structural data of PA3004-encoded protein support a physiological function as MTIP. Thus, MTI must be a metabolite in *P. aeruginosa*, but there is no previous report of MTI as a metabolite in this organism. Catabolism of [8-^{14}C]MTA in lysates

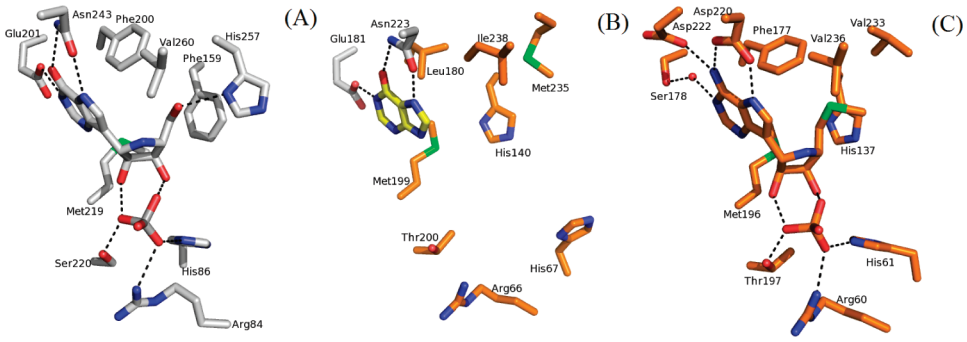

FIGURE 5: Active sites of human PNP (PDB ID 1RR6), *Pa*MTIP (PDB ID 3OZB), and human MTAP (PDB ID 1K27). (A) The conserved active site residues of human PNP in complex with ImmH are shown as sticks. The hydrogen bonds are indicated as dashed lines. ImmH is a transition state analogue inhibitor of human PNP and a mimic of inosine. (B) The active site residues of *Pa*MTIP and hypoxanthine (in yellow) are shown as sticks. The residues conserved in PNPs are colored in gray, and the residues conserved in MTAPs are colored in orange. The hydrogen bonds are indicated as dashed lines. (C) The conserved active site residues of human MTAP in complex with MT-ImmA are shown as sticks. The hydrogen bonds are indicated as dashed lines. The water molecule is drawn as a red dot. MT-ImmA is a transition-state analogue inhibitor of human MTAP and a mimic of MTA.

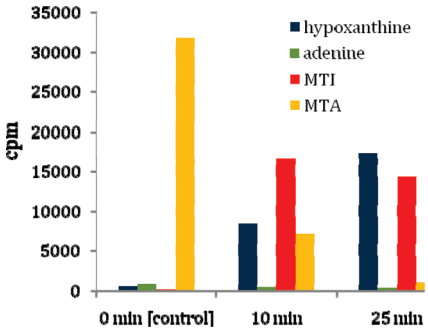

FIGURE 6: Metabolism of [8-^{14}C]MTA in *P. aeruginosa*. *P. aeruginosa* lysate was incubated with [8-^{14}C]MTA for 0, 10, and 25 min, respectively. The ^{14}C metabolites MTA, MTI, adenine, and hypoxanthine were purified using RP-HPLC and quantitated by scintillation counting.

of *P. aeruginosa* was investigated by tracking the ^{14}C-label into hypoxanthine, adenine, MTI, and MTA. If MTA is first deaminated to MTI followed by *Pa*MTIP action, the sequential conversion to [8-^{14}C]MTI and hypoxanthine would occur without adenine formation. After 10 min incubation with lysate, 77% of the MTA was converted to MTI (52%) and hypoxanthine (25%) without significant formation of adenine (Figure 6). As 98% of the total ^{14}C-label was recovered, the results establish MTA conversion to MTI and hypoxanthine but not to adenine. At 25 min incubation, over 97% of the [8-^{14}C] MTA was recovered as MTI (45%) and hypoxanthine (53%). Continuous conversion of MTA → MTI → hypoxanthine without significant MTAP or MTAN activity is supported by these results, highlighting the requirement for an MTA deaminase to catalyze the conversion of MTA to MTI. A similar pathway of MTA catabolism is found in *Plasmodium* species (*34*). The adenosine deaminase of *P. falciparum* (*Pf*ADA) deaminates adenosine and MTA as substrates with similar k_{cat}/K_m values (*32*). Its purine nucleoside phosphorylase (*Pf*PNP) also degrades inosine and MTI to hypoxanthine with similar catalytic efficiency (*31*). The substrate specificities of the *P. falciparum* enzymes permit conversion of MTA to hypoxanthine via MTI. Although MTI has been used as an MTA analogue, its function as a metabolite has been documented only in *Plasmodium* (*28*, *29*, *36*−*39*). The identification of a specific MTIP activity suggests this metabolite is more widely distributed. Homology searches using the amino acid sequence of *Pa*MTIP readily locates a large number putative of bacterial MTIPs.

Table 3: Summary of K_i Values for *Pa*MTIP and *Pf*PNP[b]

	*Pa*MTIP		*Pf*PNP[a]	
inhibitor	K_i (pM)	K_i* (pM)	K_i (nM)	K_i* (nM)
MT-ImmH	840 ± 50	76 ± 5	22 ± 3	2.7 ± 0.4
PhT-ImmH	660 ± 90	35 ± 3	150 ± 8	ND
MT-DADMe-ImmH	800 ± 100	340 ± 20	11 ± 4	0.9 ± 0.1

[a]Inhibition constants of *Pf*PNP are from Lewandowicz et al. (*42*). [b]Values are ±SE.

Picomolar Inhibitors of PaMTIP. Immucillins are transition-state analogues developed for *N*-ribosyl transferases that have ribocation character at their transition states (*40*). We tested two generations of immucillins to determine which would be the most powerful inhibitor. ImmH is a first generation immucillin, resembling early transition states as exemplified by bovine PNP (*23*) (Figure 1). DADMe-ImmH is a second generation immucillin and mimics the fully dissociated transition states of human and *P. falciparum* PNPs (*41*). 5′-Alkylthio and arylthio derivatives of two generations of immucillins (MT-ImmH, PhT-ImmH, and MT-DADMe-ImmH) have been synthesized to target the transition-state features of *Pf*PNP with MTI as the substrate (*32*). Since *Pa*MTIP catalyzes the same reaction, it would be expected that these analogues should act as transition-state analogues. The inhibitors exhibited slow-onset inhibition of *Pa*MTIP, suggesting a slow conversion of initial enzyme−inhibitor complex to a more stable conformation.

MT-ImmH inhibited *Pa*MTIP with a K_i* value of 76 pM, binding 4-fold more tightly than MT-DADMe-ImmH, suggesting that the first generation immucillins more closely resemble the transition state (Table 3). PhT-ImmH was the most tightly bound inhibitor with a K_i* value of 35 pM and demonstrates the importance of hydrophobic substituent at the 5′-position. The K_{MTI}/K_i* values were 34000 for MT-ImmH, 7600 for MT-DADMe-ImmH, and 74000 for PhT-ImmH, emphasizing the potency of these transition-state analogue inhibitors. Inhibitor specificity can be compared to that for *Pf*PNP, which catalyzes the same reaction. Thus, MT-ImmH, PhT-ImmH, and MT-DADMe-ImmH bind more weakly to *Pf*PNP with dissociation constants of 2.7, 150, and 0.9 nM, respectively (Table 3) (*31*, *42*). Binding of the bulky, hydrophobic 5′-PhT group is preferred by *Pa*MTIP where K_i* = 35 pM. This inhibitor induces slow-onset inhibition. In contrast,

the same inhibitor has K_i = 150 nM with *Pf*PNP, where it binds 4300-fold more weakly and does not induce slow-onset inhibition.

The specificity of the MTIP inhibitors of Table 3 is exceptional. None of the inhibitors gave significant inhibition with human MTAP or with *V. cholerae* MTAN. The K_i values are in excess of 10 μM for these enzymes (data not shown).

Nature of the PaMTIP Transition State. *Pf*PNP has a fully dissociated ribocation transition state with approximately 3 Å between the C1′ ribocation and N9 and a similar separation between C1′ and the attacking phosphate oxygen. Thus, it prefers to bind MT-DADMe-ImmH rather than MT-ImmH (*43*). *Pa*MTIP shows the opposite pattern, consistent with an early, dissociative transition state.

Implications for Quorum Sensing. Inhibition studies of *Pa*MTIP have identified three inhibitors with K_i* values in the picomolar range. These are candidates for blocking *Pa*MTIP activities. In most bacteria, MTAN inhibition blocks quorum sensing, but the lack of MTAN in *P. aeruginosa* indicates that *Pa*MTIP becomes an equivalent target. This study has revealed the pathway of MTA metabolism in *P. aeruginosa* and has provided new tools to explore this unusual bacterial pathway.

ACKNOWLEDGMENT

Structural data for this study were measured at beamline X29A of the National Synchrotron Light Source. Financial support comes principally from the Offices of Biological and Environmental Research and of Basic Energy Sciences of the U.S. Department of Energy and from the National Center for Research Resources of the National Institutes of Health. The authors acknowledge the Carbohydrate Chemistry Team of Industrial Research Ltd. (Lower Hutt, New Zealand) for supplying transition state analogue inhibitors.

REFERENCES

1. Hardalo, C., and Edberg, S. C. (1997) *Pseudomonas aeruginosa*: assessment of risk from drinking water. *Crit. Rev. Microbiol. 23*, 47–75.
2. Bodey, G. P., Bolivar, R., Fainstein, V., and Jadeja, L. (1983) Infections caused by *Pseudomonas aeruginosa*. *Rev. Infect. Dis. 5*, 279–313.
3. Strateva, T., and Yordanov, D. (2009) *Pseudomonas aeruginosa*—a phenomenon of bacterial resistance. *J. Med. Microbiol. 58*, 1133–1148.
4. Lyczak, J. B., Cannon, C. L., and Pier, G. B. (2002) Lung infections associated with cystic fibrosis. *Clin. Microbiol. Rev. 15*, 194–222.
5. Govan, J. R., and Deretic, V. (1996) Microbial pathogenesis in cystic fibrosis: mucoid *Pseudomonas aeruginosa* and *Burkholderia cepacia*. *Microbiol. Rev. 60*, 539–574.
6. Wagner, V. E., Bushnell, D., Passador, L., Brooks, A. I., and Iglewski, B. H. (2003) Microarray analysis of *Pseudomonas aeruginosa* quorum-sensing regulons: effects of growth phase and environment. *J. Bacteriol. 185*, 2080–2095.
7. Schuster, M., Lostroh, C. P., Ogi, T., and Greenberg, E. P. (2003) Identification, timing, and signal specificity of *Pseudomonas aeruginosa* quorum-controlled genes: a transcriptome analysis. *J. Bacteriol. 185*, 2066–2079.
8. Hentzer, M., Wu, H., Andersen, J. B., Riedel, K., Rasmussen, T. B., Bagge, N., Kumar, N., Schembri, M. A., Song, Z., Kristoffersen, P., Manefield, M., Costerton, J. W., Molin, S., Eberl, L., Steinberg, P., Kjelleberg, S., Hoiby, N., and Givskov, M. (2003) Attenuation of *Pseudomonas aeruginosa* virulence by quorum sensing inhibitors. *EMBO J. 22*, 3803–3815.
9. Rumbaugh, K. P., Griswold, J. A., Iglewski, B. H., and Hamood, A. N. (1999) Contribution of quorum sensing to the virulence of *Pseudomonas aeruginosa* in burn wound infections. *Infect. Immun. 67*, 5854–5862.
10. Smith, R. S., Harris, S. G., Phipps, R., and Iglewski, B. (2002) The *Pseudomonas aeruginosa* quorum-sensing molecule *N*-(3-oxododecanoyl)homoserine lactone contributes to virulence and induces inflammation *in vivo*. *J. Bacteriol. 184*, 1132–1139.
11. Pearson, J. P., Feldman, M., Iglewski, B. H., and Prince, A. (2000) *Pseudomonas aeruginosa* cell-to-cell signaling is required for virulence in a model of acute pulmonary infection. *Infect. Immun. 68*, 4331–4334.
12. Wu, H., Song, Z., Givskov, M., Doring, G., Worlitzsch, D., Mathee, K., Rygaard, J., and Hoiby, N. (2001) *Pseudomonas aeruginosa* mutations in *lasI* and *rhlI* quorum sensing systems result in milder chronic lung infection. *Microbiology 147*, 1105–1113.
13. Storey, D. G., Ujack, E. E., Rabin, H. R., and Mitchell, I. (1998) *Pseudomonas aeruginosa lasR* transcription correlates with the transcription of *lasA*, *lasB*, and *toxA* in chronic lung infections associated with cystic fibrosis. *Infect. Immun. 66*, 2521–2528.
14. Erickson, D. L., Endersby, R., Kirkham, A., Stuber, K., Vollman, D. D., Rabin, H. R., Mitchell, I., and Storey, D. G. (2002) *Pseudomonas aeruginosa* quorum-sensing systems may control virulence factor expression in the lungs of patients with cystic fibrosis. *Infect. Immun. 70*, 1783–1790.
15. Smith, R. S., and Iglewski, B. H. (2003) *Pseudomonas aeruginosa* quorum sensing as a potential antimicrobial target. *J. Clin. Invest. 112*, 1460–1465.
16. Gutierrez, J. A., Crowder, T., Rinaldo-Matthis, A., Ho, M.-C., Almo, S. C., and Schramm, V. L. (2009) Transition state analogs of 5′-methylthioadenosine nucleosidase disrupt quorum sensing. *Nat. Chem. Biol. 5*, 251–257.
17. Parsek, M. R., Val, D. L., Hanzelka, B. L., Cronan, J. E., Jr., and Greenberg, E. P. (1999) Acyl homoserine-lactone quorum-sensing signal generation. *Proc. Natl. Acad. Sci. U.S.A. 96*, 4360–4365.
18. Winsor, G. L., Lo, R., Sui, S. J., Ung, K. S., Huang, S., Cheng, D., Ching, W. K., Hancock, R. E., and Brinkman, F. S. (2005) *Pseudomonas aeruginosa* Genome Database and PseudoCAP: facilitating community-based, continually updated, genome annotation. *Nucleic Acids Res. 33*, D338–343.
19. Sekowska, A., Denervaud, V., Ashida, H., Michoud, K., Haas, D., Yokota, A., and Danchin, A. (2004) Bacterial variations on the methionine salvage pathway. *BMC Microbiol. 4*, 9.
20. Singh, V., Lee, J. E., Nunez, S., Howell, P. L., and Schramm, V. L. (2005) Transition state structure of 5′-methylthioadenosine/*S*-adenosylhomocysteine nucleosidase from *Escherichia coli* and its similarity to transition state analogues. *Biochemistry 44*, 11647–11659.
21. Miles, R. W., Tyler, P. C., Furneaux, R. H., Bagdassarian, C. K., and Schramm, V. L. (1998) One-third-the-sites transition-state inhibitors for purine nucleoside phosphorylase. *Biochemistry 37*, 8615–8621.
22. Singh, V., Evans, G. B., Lenz, D. H., Mason, J. M., Clinch, K., Mee, S., Painter, G. F., Tyler, P. C., Furneaux, R. H., Lee, J. E., Howell, P. L., and Schramm, V. L. (2005) Femtomolar transition state analogue inhibitors of 5′-methylthioadenosine/*S*-adenosylhomocysteine nucleosidase from *Escherichia coli*. *J. Biol. Chem. 280*, 18265–18273.
23. Morrison, J. F., and Walsh, C. T. (1988) The behavior and significance of slow-binding enzyme inhibitors. *Adv. Enzymol. Relat. Areas Mol. Biol. 61*, 201–301.
24. (1994) The CCP4 suite: programs for protein crystallography, *Acta Crystallogr., Sect. D: Biol. Crystallogr.* 50, 760−763.
25. Adams, P. D., Afonine, P. V., Bunkoczi, G., Chen, V. B., Davis, I. W., Echols, N., Headd, J. J., Hung, L. W., Kapral, G. J., Grosse-Kunstleve, R. W., McCoy, A. J., Moriarty, N. W., Oeffner, R., Read, R. J., Richardson, D. C., Richardson, J. S., Terwilliger, T. C., and Zwart, P. H. (2010) PHENIX: a comprehensive Python-based system for macromolecular structure solution. *Acta Crystallogr., Sect. D: Biol. Crystallogr. 66*, 213–221.
26. Emsley, P., and Cowtan, K. (2004) Coot: model-building tools for molecular graphics. *Acta Crystallogr., Sect. D: Biol. Crystallogr. 60*, 2126–2132.
27. Potterton, E., Briggs, P., Turkenburg, M., and Dodson, E. (2003) A graphical user interface to the CCP4 program suite. *Acta Crystallogr., Sect. D: Biol. Crystallogr. 59*, 1131–1137.
28. Carteni-Farina, M., Oliva, A., Romeo, G., Napolitano, G., De Rosa, M., Gambacorta, A., and Zappia, V. (1979) 5′-Methylthioadenosine phosphorylase from *Caldariella acidophila*. Purification and properties. *Eur. J. Biochem. 101*, 317–324.
29. Zappia, V., Oliva, A., Cacciapuoti, G., Galletti, P., Mignucci, G., and Carteni-Farina, M. (1978) Substrate specificity of 5′-methylthioadenosine phosphorylase from human prostate. *Biochem. J. 175*, 1043–1050.
30. Stoeckler, J. D., Cambor, C., Kuhns, V., Chu, S. H., and Parks, R. E., Jr. (1982) Inhibitors of purine nucleoside phosphorylase, C(8) and C(5′) substitutions. *Biochem. Pharmacol. 31*, 163–171.

31. Shi, W., Ting, L.-M., Kicska, G. A., Lewandowicz, A., Tyler, P. C., Evans, G. B., Furneaux, R. H., Kim, K., Almo, S. C., and Schramm, V. L. (2004) *Plasmodium falciparum* purine nucleoside phosphorylase: crystal structures, immucillin inhibitors, and dual catalytic function. *J. Biol. Chem. 279*, 18103–18106.
32. Ting, L.-M., Shi, W., Lewandowicz, A., Singh, V., Mwakingwe, A., Birck, M. R., Ringia, E. A. T., Bench, G., Madrid, D. C., Tyler, P. C., Evans, G. B., Furneaux, R. H., Schramm, V. L., and Kim, K. (2005) Targeting a novel *Plasmodium falciparum* purine recycling pathway with specific immucillins. *J. Biol. Chem. 280*, 9547–9554.
33. Ho, M. C., Shi, W., Rinaldo-Matthis, A., Tyler, P. C., Evans, G. B., Clinch, K., Almo, S. C., and Schramm, V. L. (2010) Four generations of transition-state analogues for human purine nucleoside phosphorylase. *Proc. Natl. Acad. Sci. U.S.A. 107*, 4805–4812.
34. Stoeckler, J. D., Poirot, A. F., Smith, R. M., Parks, R. E., Jr., Ealick, S. E., Takabayashi, K., and Erion, M. D. (1997) Purine nucleoside phosphorylase. 3. Reversal of purine base specificity by site-directed mutagenesis. *Biochemistry 36*, 11749–11756.
35. Murkin, A. S., Clinch, K., Mason, J. M., Tyler, P. C., and Schramm, V. L. (2008) Immucillins in custom catalytic-site cavities. *Bioorg. Med. Chem. Lett. 18*, 5900–5903.
36. Ferro, A. J., Barrett, A., and Shapiro, S. K. (1976) Kinetic properties and the effect of substrate analogues on 5′-methylthioadenosine nucleosidase from *Escherichia coli*. *Biochim. Biophys. Acta 438*, 487–494.
37. Guranowski, A. B., Chiang, P. K., and Cantoni, G. L. (1981) 5′-Methylthioadenosine nucleosidase. Purification and characterization of the enzyme from *Lupinus luteus* seeds. *Eur. J. Biochem./FEBS 114*, 293–299.
38. Cornell, K. A., Swarts, W. E., Barry, R. D., and Riscoe, M. K. (1996) Characterization of recombinant *Eschericha coli* 5′-methylthioadenosine/*S*-adenosylhomocysteine nucleosidase: analysis of enzymatic activity and substrate specificity. *Biochem. Biophys. Res. Commun. 228*, 724–732.
39. White, M. W., Vandenbark, A. A., Barney, C. L., and Ferro, A. J. (1982) Structural analogs of 5′-methylthioadenosine as substrates and inhibitors of 5′-methylthioadenosine phosphorylase and as inhibitors of human lymphocyte transformation. *Biochem. Pharmacol. 31*, 503–507.
40. Evans, G. B., Furneaux, R. H., Gainsford, G. J., Schramm, V. L., and Tyler, P. C. (2000) Synthesis of transition state analogue inhibitors for purine nucleoside phosphorylase and *N*-riboside hydrolases. *Tetrahedron 56*, 3053–3062.
41. Evans, G. B., Furneaux, R. H., Lewandowicz, A., Schramm, V. L., and Tyler, P. C. (2003) Synthesis of Second-Generation Transition State Analogues of Human Purine Nucleoside Phosphorylase. *J. Med. Chem. 46*, 5271–5276.
42. Lewandowicz, A., Ringia, E. A. T., Ting, L.-M., Kim, K., Tyler, P. C., Evans, G. B., Zubkova, O. V., Mee, S., Painter, G. F., Lenz, D. H., Furneaux, R. H., and Schramm, V. L. (2005) Energetic mapping of transition state analogue interactions with human and *Plasmodium falciparum* purine nucleoside phosphorylases. *J. Biol. Chem. 280*, 30320–30328.
43. Lewandowicz, A., and Schramm, V. L. (2004) Transition state analysis for human and *Plasmodium falciparum* purine nucleoside phosphorylases. *Biochemistry 43*, 1458–1468.